SnO2 "Russian Doll" octahedra prepared by metalorganic synthesis: A new structure for sub-ppm CO detection

Justyna Jońca, Andrey Ryzhikov, Myrtil L. Kahn, Katia Fajerwerg, Audrey Chapelle, Philippe Menini, Pierre Fau

SnO_2 "Russian Doll" Octahedra Prepared by Metalorganic Synthesis: A New Structure for sub-ppm CO Detection

Justyna Jońca,[a] Andrey Ryzhikov [a], Myrtil L. Kahn * [a], Katia Fajerwerg [a, b], Audrey Chapelle [c], Philippe Menini [b, c], Pierre Fau * [a, b]

Abstract: Micrometer-sized hierarchical $Sn_3O_2(OH)_2$ octahedra which are self-assembled one inside the other, similarly to "Russian-doll" organization, have been obtained by a metalorganic approach. This synthesis is based on the controlled hydrolysis of $[Sn(NMe)_2]_2$ compound in the presence of an alkylamine ligand in an organic solvent (THF). The water level turns to be a key parameter for the formation of these multi-walled octahedra. These structures have been used as gas sensitive layers on micromachined silicon devices. During *in situ* heating, $Sn_3O_2(OH)_2$ oxidizes into SnO_2 while retaining the initial morphology. The sensors present an outstanding dynamic response at very low CO concentrations (7% and 67% of resistance variation to respectively 0.25 and 20 ppm CO, for an operating temperature of 500°C).This superior gas sensing performance is closely related to the unique microstructure of these SnO_2 multi-walled octahedra.

Introduction

Nanostructures of SnO_2 including nanoparticles,[1] nanowires,[2] nanobelts,[3] and nanotubes[4, 5] have been widely used in many fields, such as gas sensors,[1, 4] solar cells,[3] and lithium batteries.[1, 5] Recently, hierarchical and/or hollow SnO_2 micro- and nanostructures have attracted much interest because of their widespread potential applications, including gas sensors.[6] Indeed, they have shown enhanced sensitivity toward gases, especially ethanol, as compared to simple nanostructures or thin films.[7-10]

Several growth processes have been proposed for the preparation of such complex structures. Templating procedures have been considered as the most straightforward methods. They involve the controlled assembly of the chosen material on various removable "hard" templates such as silica, carbon and polymers. For example, uniform hollow spheres have been obtained through SnO_2 film deposition on polyelectrolyte modified SiO_2 spheres acting as template.[11] Wu et al. reported on the synthesis of carbon-coated SnO_2 (SnO_2–C) nanotubes through a simple glucose hydrothermal and subsequent carbonization approach, by using Sn nanorods as sacrificial templates.[12] The main drawbacks of this method are generally the difficulty to completely eliminate the template and the limited capacity to produce large-scale syntheses. Therefore, it is highly desirable to develop new strategies for the facile synthesis of hollow nanostructures. One strategy is to replace "hard" templates by "soft" ones such as micelles. For example, tin oxide hollow nanospheres have been successfully synthesized from mixed ethanol and water systems containing sodium dodecyl benzenesulfonate (SDBS) and terephthalic acid as surfactants.[13] Template-free routes have also attracted considerable interest. For example, SnO_2 polyhedra with hollow structures have been synthesized in water through a two-step oriented attachment mechanism.[14] The as-synthesized SnO_2 nanocrystallites (3-5 nm) are assembled in solution into bidimensional triangular sheets, which in turn self-assemble into tridimensional hollow octahedral structures. In another approach, an hydrothermal route has led to the formation of hierarchical SnO_2 microspheres, built from self-assembled one-dimensional SnO_2 nanorods, through Ostwald ripening process.[9] Yin et al. have prepared SnO_2 hollow octahedra assembled from nanorods arrays through removal of Zn^{2+} ions from $ZnSn(OH)_6$ precursor by ammonia.[15] Hierarchical hollow SnO_2 microspheres have been also prepared *via* Ostwald ripening method, by an hydrothermal route using NaF as morphology controlling agent.[16] To the best of our knowledge, no example of multi-walled SnO_2 octahedra structures has been reported, even if hierarchical solid or hollow SnO_2 structures have been described.[6-11], [14-16]

In this paper, we describe the synthesis of multi-walled hierarchical $Sn_3O_2(OH)_2$ octahedra powders by the controlled hydrolysis of $[Sn(NMe_2)_2]_2$ in the presence of hexadecylamine (HDA). During the synthesis, initial nanoparticles self-assemble into triangular sheets and planar coalescence of these "units" finally leads to the formation of three-dimensional porous octahedra. Interestingly, these octahedra exhibit a multi-walled structure. Unlike other synthetic methods,[14, 15] the preparation of these octahedra has been done at room temperature and under atmospheric pressure, using standard Schlenk tube technique. These powders have been dispersed in a solvent and drop-deposited on silicon chips for gas detection purpose. After *in situ* heating under ambient air at 500°C, $Sn_3O_2(OH)_2$ is transformed into SnO_2, while retaining the initial morphology. The sensors response to different gases, such as CO, C_3H_8, NH_3, and NO_2 has been measured. Unprecedented gas responses down to 0.25 ppm CO have been measured, and a resistance variation of 55% is obtained with a CO level as low as 10 ppm. Such a high dynamic response to low CO levels suggests the possibility to build a new class of device applied to the detection of low CO range. Additionally, the performance comparison with SnO_2 nanoparticles and thin-film sensors highlights the superior gas sensing properties of these hierarchical octahedra. The outstanding sensitivity of the devices is ascribed to the unique multi-walled microstructure of tin oxide nanoparticles.

Results and Discussion

[a] Dr. Justyna Jońca, Dr. Andrey Ryzhikov, Dr. Myrtil L. Kahn, Dr. Katia Fajerwerg, Dr. Pierre Fau
Laboratoire de Chimie de Coordination (LCC), CNRS
205 route de Narbonne
31077 Toulouse Cedex 4, France
E-mail: pierre.fau@lcc-toulouse.fr, myrtil.kahn@lcc-toulouse.fr
[b] Dr. Katia Fajerwerg, Dr. Philippe Menini, Dr. Pierre fau
Université Fédérale de Toulouse, UT III Paul Sabatier
118 route de Narbonne
31062 Toulouse Cedex 9, France
[c] Dr. Audrey Chapelle, Dr. Philippe Menini
Laboratoire d'Analyse et d'Architecture des Systèmes (LAAS)
7 Avenue du Colonel Roche
31400 Toulouse, France

Samples have been prepared by a one-pot metalorganic approach developed in our team for metal oxide synthesis.[18, 19] The method is based on the controlled hydrolysis of a halide-free precursor, $[Sn(NMe_2)_2]_2$, by humidified THF in the presence of HDA at room temperature and under argon atmosphere. In these conditions, a white powder spontaneously forms in the reactor after few minutes, and the reaction is left to continue during 16 hours. Afterwards, organic ligands (HDA), which may play a detrimental role in the performance of gas sensitive layer, are eliminated from the powder by a triple washing in acetone followed by centrifugation steps (described in experimental section). The efficiency of the washing procedure is evidenced by ATR-IR analyses (Figure S1). IR bands corresponding to HDA compound are observed on the spectrum of the as-prepared powder. After the washing step, the Sn-O vibration band (539 cm^{-1}) is detected, while the HDA bands have almost fully disappeared.

Morphology and chemical composition

The crystallographic structure of the as-prepared powder have been determined by X-ray diffraction analyses (**Figure 1**a). The sample presents a tetragonal symmetry (space group $P4_12_1c$, a_o=7.9269, c_o=9.0970 Å, JCPDS No. 00-055-0838), which is fully assigned to hydroromarchite $Sn_3O_2(OH)_2$ structure.[20] XRD analyses of the powder calcined at 250°C and 450°C in ambient air are reported on Figure 1b and Figure 1c, respectively. After calcination at 250°C, peaks at 29.9° (2Θ) and at 33.3, 47.8, 50.9, and 57.8° are observed. These peaks are characteristic of the (101), (110), (200), (112) and (211) planes of the tetragonal SnO structure (JCPDS No. 00-001-0902).[21] Two extra peaks are present which do not correspond to SnO structure (at 2Θ = 28° and 52°). These peaks may originate from an intermediate structure between $Sn_3O_2(OH)_2$ and SnO. At a higher calcination temperature (450°C), a new diffraction pattern, characteristic of the tetragonal SnO_2 structure (JCPDS No. 01-071-5324), is evidenced.[22] The controlled hydrolysis of $[(Sn(NMe_2)_2]_2$ under argon leads to the formation of $Sn_3O_2(OH)_2$ phase, which can easily be transformed into SnO_2 by a simple calcination under air. The Field Emission Scanning Electron Microscopy (FESEM) image of washed powder prepared with 8 eq. H_2O and 0.1 eq. HDA is presented in **Figure 2**a. The $Sn_3O_2(OH)_2$ powder presents micron size and very well defined octahedral structures. The size of these octahedra, estimated by the length of their base, varies from 0.5 to 6 µm (average 2.7 ± 1.3 µm). A highly porous structure is evidenced on some octahedra presenting large openings on apexes of the structure (Figure 2b). It is noteworthy that the morphology of the as-prepared octahedra is maintained even after calcination at 500°C (Figure 2c, 2d). Furthermore, some fully opened octahedra reveal a “Russian doll” structure, where several octahedra are nested into each other (figure 2c).

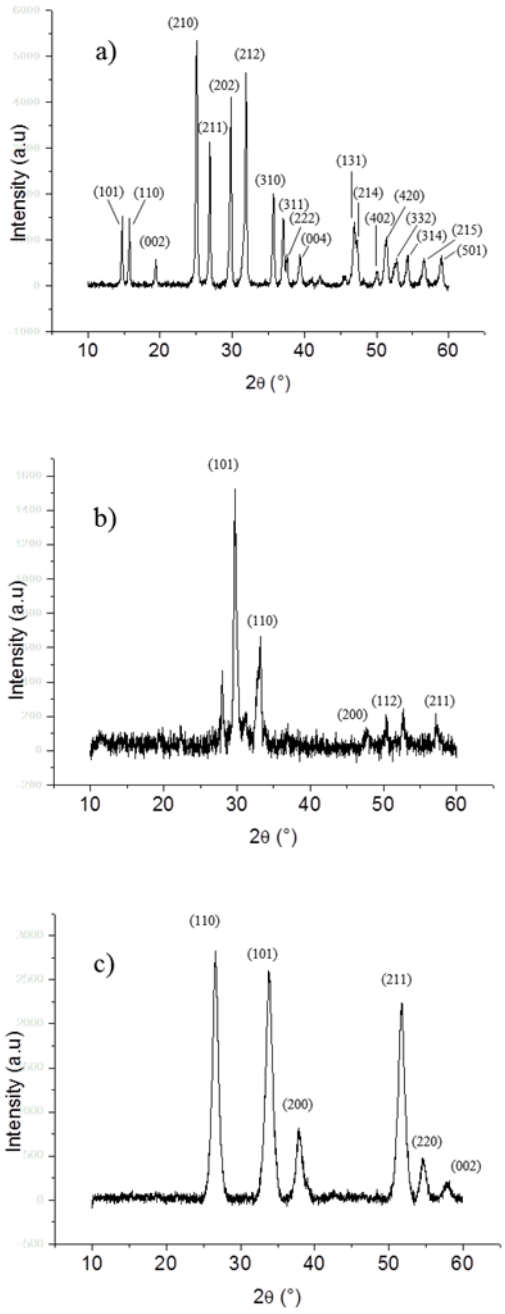

Figure 1. X-ray diffraction patterns of octahedra powder: $Sn_3O_2(OH)_2$ structure obtained at room temperature (a), SnO structure obtained after calcination at 250°C (b) SnO_2 structure obtained at 450°C (c).

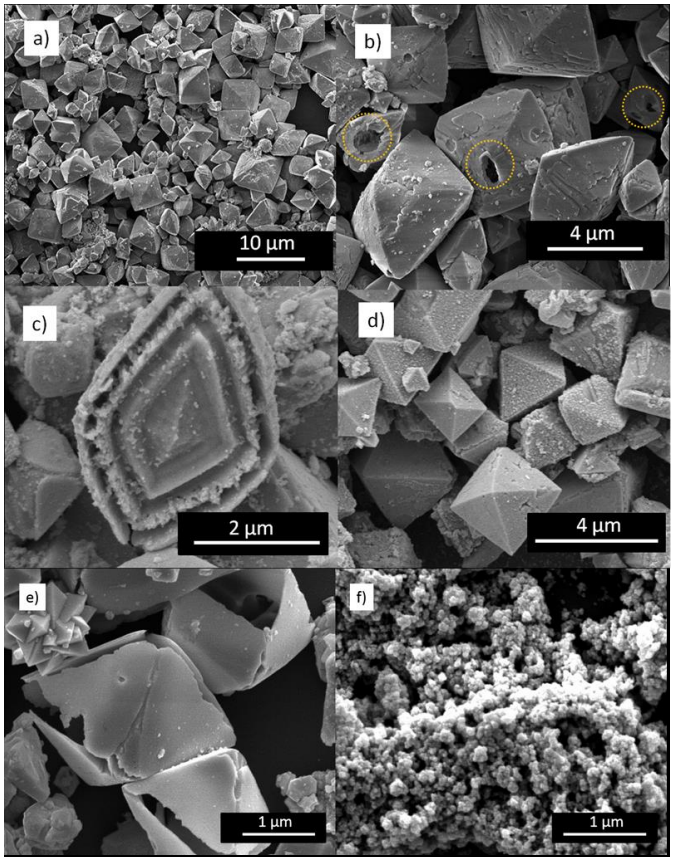

Figure 2. FESEM images of the $Sn_3O_2(OH)_2$ octahedra prepared with 8 eq H_2O (a-d), $Sn_3O_2(OH)_2$ crystals presenting an open porosity (b), SnO_2 opened crystal presenting "Russian-doll" structure (c) and SnO_2 sensitive layer on sensor device after *in situ* heating at 500°C (d), $Sn_3O_2(OH)_2$ octahedra formed with 4 eq. H_2O (e), $Sn_3O_2(OH)_2$ aggregates formed with 2 eq. H_2O (f).

The walls thickness of these unique structures is in the range of 60 to 180 nm. The inner walls are separated from each other by around 300 to 350 nm. However, it is difficult to provide some statistical data on these latter parameters owing to the presence of only few opened structures with measurable walls separation distance and thickness. Anyway, these porous and multi-walled structures offer numerous gateways for gaseous exchanges between the inner and outer walls, which is of key interest for gas sensors applications.[23] Interestingly, the outer shape and crystal size are comparable to single-walled hollow octahedra prepared by another approach based on hydrothermal decomposition of SnF_2 at 180°C in an autoclave.[14] However, our halide-free process takes advantage of the high reactivity of the metalorganic complex under mild conditions, and is performed at room temperature and under atmospheric pressure in a simple Schlenk tube. The amount of water used for the hydrolysis of the tin precursor has a major influence on the $Sn_3O_2(OH)_2$ morphology. When the water amount is decreased from 8 eq. to 4 eq., a mix of aggregates and octahedra is observed. In the latter case, the octahedra appear rather uncompleted, some of them present either missing or loose facets and the entirely hollow structure of the crystals is easily observed (Figure 2e). The size of these octahedra, is similar to the one formed with 8 eq. of water (Figure 2a-d) and varies from 0.7 to 6 µm (average 2.6 ± 1.5 µm). The wall thickness seems also similar, with a size around 80 to 160 nm. When the amount of water is 2 eq., the self-assembly process is lost, and only aggregated $Sn_3O_2(OH)_2$ nanoparticles are formed (Figure 2f). The increase of the amount of HDA to 1 eq. does not significantly influence on the $Sn_3O_2(OH)_2$ octahedra morphology. However, the complete absence of amine ligand leads to the growth of shapeless aggregates that are only scarcely soluble in THF (Figure S2). Therefore, the presence of an alkylamine, in combination with sufficiently humidified THF solvent, is a key parameter to control the multi-walled octahedra assembly formation. Nitrogen adsorption-desorption measurements performed on both $Sn_3O_2(OH)_2$ octahedra and nanoparticles give surface areas of 19 $m^2.g^{-1}$ and 105 $m^2.g^{-1}$, respectively (Figure S3).

Formation of $Sn_3O_2(OH)_2$ octahedra

In order to better understand the growth process of the $Sn_3O_2(OH)_2$ octahedra, time-dependent syntheses have been carried out. The TEM images reveal that a large number of self-assembled triangular sheets are rapidly formed within 5-10 minutes of reaction (**Figure 3**a). Some octahedral crystals are also already observed. After 1 hour, 3 hours and 7 hours of reaction, some triangular sheets are still present on the TEM images (Figure 3b). Their quantity is rapidly decreasing with reaction time and after 16 hours the sample only presents octahedra (Figure 3c). Further HRTEM investigations of the $Sn_3O_2(OH)_2$ octahedra have evidenced their polycrystalline character and revealed a hierarchical structuration. Indeed, both self-assembled triangular sheets and octahedral crystals are built by the self-assembly of initial nanoparticles with a diameter of 3.9 ± 0.9 nm (Figures 3d, 3e). These nanoparticles result from the hydrolysis of $[Sn(NMe_2)_2]_2$ in the presence of HDA. The stabilizing and growth orienting properties of alkylamines are known to produce well defined nanostructures of various metal oxides such as ZnO, NiO, γ-Fe_2O_3, or FeO by the metalorganic approach.[18, 19] Additionally, the bonding of alkylamine ligands to metal oxide surface has been evidenced by NMR spectroscopy.[24] This suggests that the building process starts by the formation of $Sn_3O_2(OH)_2$ nanoparticles stabilized by HDA, which self-assemble by an oriented attachment process into triangular polycrystalline planes in solution.[25-28] Further coalescence of the triangular sheets leads to the tridimensional construction of octahedra. Therefore, the hierarchical $Sn_3O_2(OH)_2$ octahedra of this study can be described as supercrystalline microstructure. Some authors have already reported on the facile formation of tin dioxide octahedra obtained by the hydrolysis of tin precursors.[14, 29] The evolution towards octahedral shape seems to follow a thermodynamically favorable path. Nevertheless, this process evolution requires several necessary reaction conditions. For example, single-walled hierarchical hollow SnO_2 octahedra have been prepared by the hydrolysis of a tin halide compound.[14] According to these authors, the addition of ethylenediamine, in combination with a mixture of 2-propanol and water, is crucial for the stabilization of triangular sheets of SnO_2, while maintaining the small crystalline size. However, this synthesis is conducted at high temperature (180°C) in a large excess of water as the main

solvent of the system. Our synthetic method, conducted at room temperature, is based on the complementary presence of an alkylamine and of low and controlled amount of water in the organic solvent phase. Therefore, we highlight here the interplay role of HDA in combination with the THF/water ratio, that control the assembly of primary $Sn_3O_2(OH)_2$ octahedra. Indeed, when the amount of water is too low, no triangular sheets are formed, and only $Sn_3O_2(OH)_2$ aggregated nanoparticles are obtained (Figure 2f).

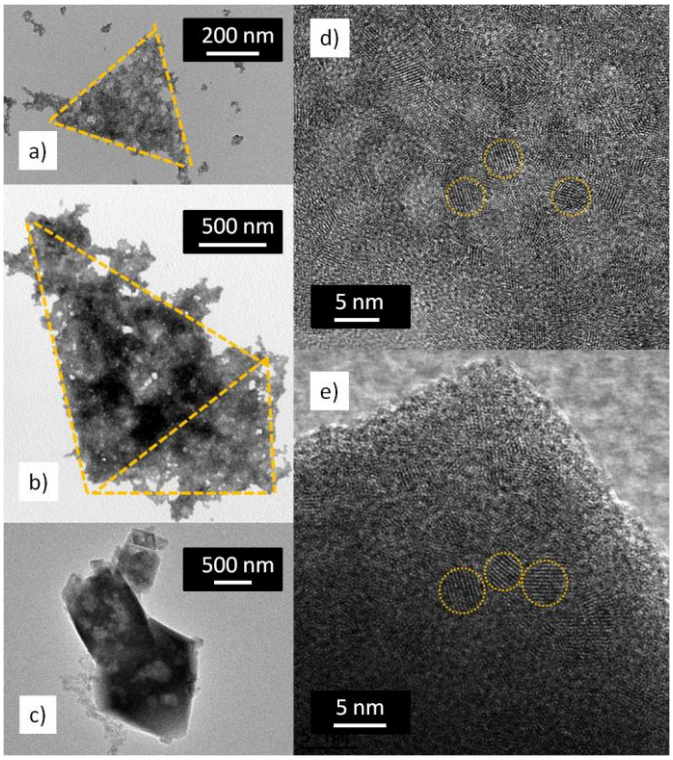

Figure 3. TEM image of $Sn_3O_2(OH)_2$ triangular sheets after 5 min (a) and 7h (b) of reaction, HRTEM image of the $Sn_3O_2(OH)_2$ octahedra obtained after 16h of reaction (c), HRTEM image of $Sn_3O_2(OH)_2$ nanocrystalline triangular sheets (d), HRTEM image of $Sn_3O_2(OH)_2$ nanocrystalline octahedra facet (e).

Therefore, an accurate amount of water not only ensures the complete hydrolysis of tin precursor into $Sn_3O_2(OH)_2$ nanoparticles, but also participates in the formation and assembly of triangular sheets. The ratio of THF to water level also plays a key role in the nesting of the octahedra, since in medium level water conditions (4 eq.), single-walled octahedra are obtained. Amphiphilic molecules are known to form complex assemblies such as onion-like structures in an appropriate water to amphiphilic molecules ratio.[30] In our case, the amphiphilic species could be composed by the hydrophilic $Sn_3O_2(OH)_2$ moiety, and by the hydrophobic alkyl chain of HDA. The multi-walled particles formation could result from the interactions between water and these amphiphilic species. Interactions such as hydrogen bonding involving water, amines, and THF molecules may be involved in the multi-walled structures formation. However, such a complex structuration requires a more detailed study, and theoretical support.[31] This study is under investigation.

Comparison of gas sensing properties of different SnO_2 microstructures (octahedra, nanoparticles and thin film)

The multi-walled hierarchical octahedra synthesized in this work could find application in several fields (*e.g.* gas sensing, solar cells, or lithium batteries). It is particularly expected that such a microstructure might bring about optimized gas sensing properties.[7-10] Our "Russian doll" octahedra have been used for the preparation of gas sensing devices, and compared with simple sensitive layers made of SnO_2 nanoparticles (prepared with 2 eq. H_2O, Figure 2f), or SnO_2 sputtered thin films (commercial source, grain diameter *ca.* 500 nm, thickness *ca.* 250 nm, Figure S4). The response of octahedra gas sensors to 100 - 490 ppm CO, 100 - 400 ppm C_3H_8, 5 ppm NH_3, and 1 ppm NO_2, operated at various temperatures, are reported on **Figure 4** a-d. It is noteworthy that the sensors have shown high and reversible responses to all gases. The normalized responses of the sensors operated at different temperatures are presented on Figure 4e. The response to 100 ppm CO increases with the operating temperature and reaches its maximum value at 500°C (Rn= 65%). For high CO concentrations (100-490 ppm), octahedra and nanoparticles present a quite similar response level (**Table 1**). However, due to their nanosized structure, they exhibit a 1.2-1.5 – fold increase in sensitivity compared to SnO_2 thin film. The maximum sensitivity to 100 ppm C_3H_8 has been obtained at about 500°C for all sensors. The SnO_2 octahedra and nanoparticles give similar normalized responses to this gas (Rn= 56% and 61%, respectively), which represent an increase of around 2.7 fold, compared to SnO_2 thin film. Interestingly, the response improvement for octahedra seems to be even more marked in the case of low amounts of reacting gases. The SnO_2 octahedra and nanoparticles show a strong response to 5 ppm NH_3 at 500°C (Rn= 41% and 33%, respectively).The sputtered thin film sensors are not sensitive to such amount of NH_3. The SnO_2 octahedra show a very high response to 1 ppm NO_2 (Rn=196%) at low operating temperature (300°C). Comparatively, in the same conditions, the SnO_2 nanoparticles are less sensitive (Rn=28%), and the thin film SnO_2 sensors show no response at all. These results suggest the high potential of SnO_2 octahedra for the detection of gases at a very low concentration.

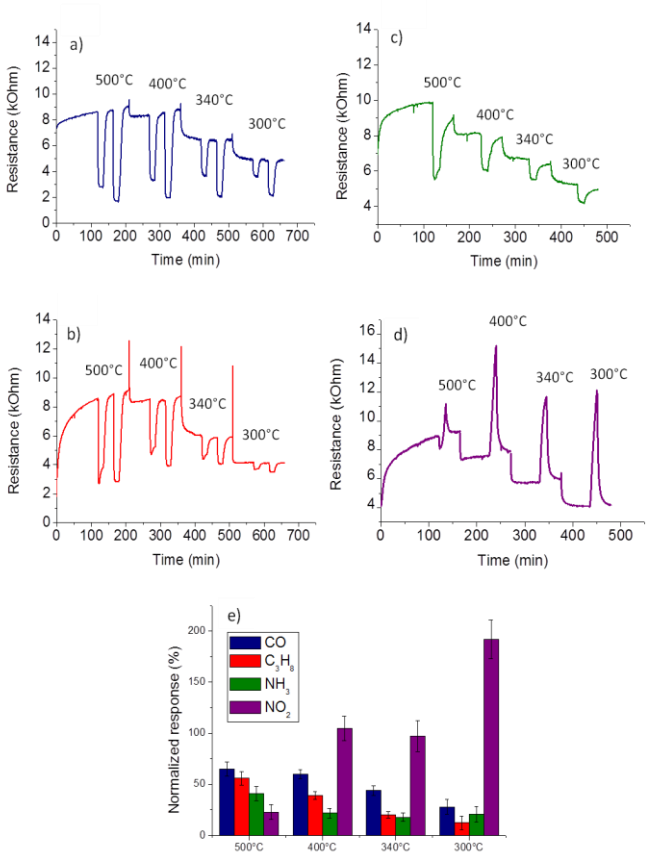

Figure 4. Responses of SnO_2 octahedra sensors to 100 and 490 ppm CO (a), 100 and 400 ppm C_3H_8 (b), 5 ppm NH_3 (c), 1 ppm NO_2 (d), and comparison of octahedra SnO_2 sensors normalized responses to 100 ppm CO, 100 ppm C_3H_8, 5 ppm NH_3 and 1 ppm NO_2, at different temperatures (due to short exposure time, NO_2 responses are transitory, they are presented here as indicative values compared to the steady state responses to reducing gasses) (e).

Table 1. Comparison of normalized responses of SnO_2 octahedra, nanoparticles and thin film to 100, 250 and 490 ppm CO, 100 ppm C_3H_8, 5 ppm NH_3 and 1 ppm NO_2.

Sensitive layer	100 ppm CO (500°C)	250 ppm CO (500°C)	490 ppm CO (500°C)	100 ppm C_3H_8 (500°C)	5 ppm NH_3 (500°C)	1 ppm NO_2 (300°C)
Octahedra	73%	82%	85%	56%	41%	196%
Nanoparticles	64%	72%	87%	61%	33%	28%
Thin film	47%	63%	70%	21%	0%	0%

Detection properties of SnO_2 octahedra to low CO levels

Low CO concentrations comprised between 0.25 and 490 ppm, have been investigated for the three different sensors types. Normalized responses for all sensors are presented on **Figure 5**. The SnO_2 octahedra sensors exhibit a remarkably high response to low CO concentrations compared to the nanoparticles or thin film ones (Figure 5a, 5b). Nanoparticles and thin film sensors give no response at all to 0.25 and 0.5 ppm CO, while the SnO_2 octahedra show a normalized response of 7% and 14%, respectively (**Table 2**). To the best of our knowledge, no examples of sub-ppm CO detection have been reported so far with undoped SnO_2 structures. One of the best reported sensing properties has been obtained with hierarchical flower-like SnO_2 sensors, which offer a detection limit of 5 ppm CO at an operating temperature of 320°C in dry air.[32] Thin film and nanoparticles sensors give only a very weak responses to CO in the concentration range of 1-10 ppm, with resistance variations between 3% and 13% (Table 2). In the same test conditions, the normalized responses of the SnO_2 octahedra vary from 18% to 55%, which gives a 6 to 5.5 fold increase. These sensors present an unprecedented dynamic of their response to very low CO concentration (between 0.25 to 10 ppm). The reproducibility of the high sensitivity these sensors is presented on **Figure S5**. Interestingly, the sensors response under CO starts to saturate (response threshold above 60%) at a level of 250 ppm for thin film (Rn= 63%), 100 ppm CO for the nanoparticles (Rn= 64%) and as low as 20 ppm for the SnO_2 octahedra (Rn= 67%). This very early response saturation reflects the remarkable capability of SnO_2 octahedra to detect low CO quantities.

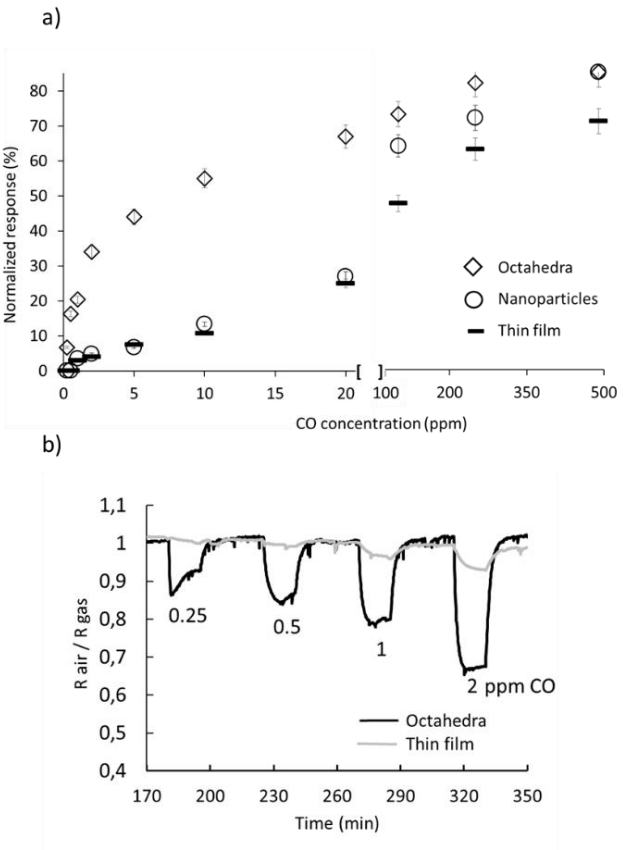

Figure 5. Normalized responses to CO for sensors at operating temperature of 500°C obtained with SnO_2 octahedra, SnO_2 nanoparticles and SnO_2 thin film sensors. Normalized responses to CO in concentration range of 0.25 – 490 ppm (a), and real time responses of thin films and octahedra to 0.25-2.0 ppm CO (b).

Table 2. Comparison of normalized responses to 0.25, 0.5, 1 and 10 ppm CO, for SnO_2 octahedra, nanoparticles and thin film.

Sensitive layer	0.25 ppm CO	0.5 ppm CO	1ppm CO	10 ppm CO
Octahedra	7%	14%	18%	55%
Nanoparticles	0%	0%	4%	13%
Thin film	0%	0%	3%	10%

Gas response improvement for SnO_2 octahedra

As mentioned above, SnO_2 octahedra present the best sensitivity and a remarkable dynamic response for very low CO amounts. The responses of SnO_2 nanoparticles lay at a mean level, whereas SnO_2 thin films exhibit the lowest sensitivity. Thin film SnO_2 sensors are based on a bi-dimensional network of relatively large grains (~500 nm) connected by their grain boundaries. The SnO_2 nanoparticles sensors are made of a network of interconnected very small grains. On the other side, the SnO_2 octahedra are built with the same elementary nanoparticles, but organized in a very particular architecture. The effect of grain size on the sensitivity has been established by several semi-quantitative models.[33, 34] According to these models, the gas sensitive layers consist of partially sintered crystallites that are connected to their neighbors by necks. These interconnected grains form larger aggregates that are connected to their neighbors by grain boundaries. Three cases are usually considered according to the relationship between the grain size (D) and the width of the depletion layer (L). The depletion layer L corresponds to an electron-trapped zone due to the adsorption of oxygen species at the grain surface. These adsorbed oxygen species directly react with CO molecules during sensing operation of the device. This depletion layer is usually found to extend to 3 to 4 nm under the surface of undoped SnO_2 grains.[35] For large grains (D>>2L), *e. g.* in the case of the thin film sensor used in this study (**Figure 6**a), the main volume of the crystallites remains unaffected by the surface interactions with the gas phase. Here, the predominant effect of the ambient gas on the sensor conductivity is introduced *via* the grain boundary barriers for intergrain charge transport. The electrical resistance of the sensor depends exponentially on the barriers height and their number. Thus, for a material with large and dense grain, the gas sensing properties are controlled by the grain boundary barriers. As the grain size decreases, the depletion region extends deeper into the grain volume and, consequently, the grain core region modified by the gaseous environment becomes active. When D is close to 2L but is still larger than 2L (D≥2L), the depletion region that surrounds each neck forms a constricted channel within each aggregate. The conductivity consequently depends not only on the grain boundary barriers, but also on the cross section area of these channels. The current constriction effect adds up to the effect of the grain boundary barriers, and therefore the gas sensitivity is enhanced with respect to the previous case. Sensitivity increases when D decreases. For very small grains (D<2L), *e.g.* in the case of the nanoparticles sensors developed in this work (Figure 6b), the depletion region extends throughout the entire grain and the crystallites are almost fully depleted of mobile charge carriers. As a result, the conductivity decreases steeply since the conduction channels between the grains have vanished. The energy bands are nearly flat throughout the whole structure of the interconnected grains, and the conductivity is controlled by the intracrystallite charge transport, *i.e.* grain controlled. The highest sensitivity, proportional to 1/D, is obtained in this case. Overall, this model explains the higher sensor signals exhibited by the SnO_2 nanoparticles and SnO_2 octahedra compared to SnO_2 thin film. However, the reason for different gas sensing properties between nanoparticles and octahedra structures cannot be provided with such an approach since both structures are constituted of the same elementary SnO_2 nano-bricks.

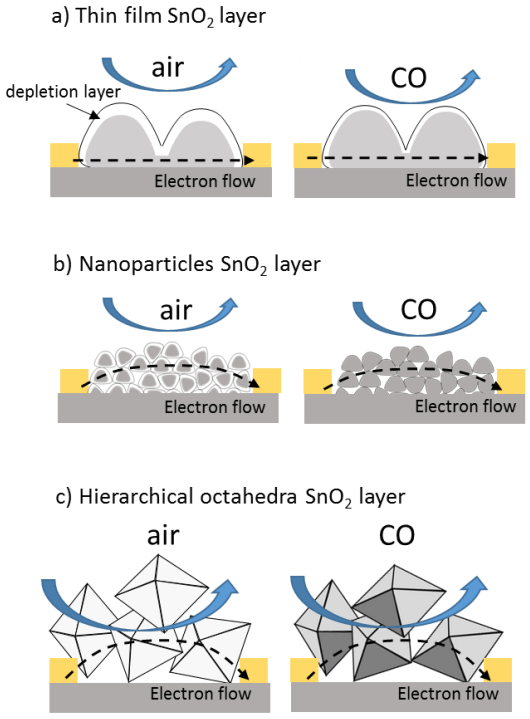

Figure 6. Schematic cartoon of the intergrains electrical modulation under air and CO exposure in thin film (a), nanoparticles (b) and octahedra (c).

The very open structure of micron-sized hierarchical structures provides a large porosity for an effective gas diffusion and a high response to low reacting gas contents.[36, 37] In a similar example, it has been recently shown that hierarchical CuO grains, which presented a low specific surface area but a large open porosity, have achieved the highest gas response to sub-ppm quantities of H_2.[36] The porosity of our sensitive layer made of SnO_2 octahedra, plays a role at three different levels: *i*) the erratic layer of micron-sized grains generates a primary porosity, *ii*) the multi-walled

structure allows the gas to diffuse inside each octahedra between their walls and *iii*) the walls of the octahedra are made porous by the self-assembly process which generates defects. In such a case, both inner and outer sides of the microstructure walls are accessible to reactive gaseous molecules.[38,39] By consequence, the entire "Russian doll" octahedra are spontaneously converted into a highly conducting state when exposed to low amounts of CO molecules (Figure 6c). In addition, according to the model developed by Barsan *et al*. for large oxide grains, [40] the sensor resistance changes are also related to the effective contact area between the grains. This model suggests that the sensor signal can be improved by changing the shape and/or dimensions of sensitive layers grains. The highest gas response improvement comes from a reduction of the effective contact area between the grains. Therefore, the superior CO detection performance of "Russian doll" SnO_2 octahedra may be also the consequence of the reduced contact area between large and porous octahedra made of nanosized particles (Figure 6c). A remarkably high gas sensitivity, at low gas concentration, is achieved by using such large, hierarchical and porous structures.

Conclusions

In summary, a simple and original procedure based on metalorganic approach has been applied in order to prepare "Russian-doll" $Sn_3O_2(OH)_2$ octahedra at room temperature and ambient pressure. The addition of HDA, combined with a controlled amount of water added in the organic medium, is responsible for the multi-walled octahedra formation. The $Sn_3O_2(OH)_2$ octahedra have been deposited on silicon chips as gas sensitive layer. After calcination at 450°C, $Sn_3O_2(OH)_2$ transforms into SnO_2 without change of the grain morphology. Gas sensing properties of the SnO_2 octahedra to CO, C_3H_8, NH_3, and NO_2 gases have been investigated at different operating temperatures. At 500°C, the sensors show an unprecedented detection dynamic to CO in the range of 0.25 to 10 ppm with 7% and 55% of resistance variation, respectively. Moreover, the comparison between various SnO_2 microstructures (octahedra, nanoparticles, thin film layers) highlights the superior gas sensing properties of these hierarchical octahedra. These remarkable gas sensing properties are associated with this unique structure. They can be applied in the further development of a new class of gas sensors dedicated to sub-ppm level gas detection.

Experimental Section

Synthetic procedures

The synthesis of tin hydroxide has been performed at room temperature and under argon atmosphere in standard Schlenk tubes. Bis(dimethylamido)tin(II), $[(Sn(NMe_2)_2]_2$ (NanoMePS) is used as metalorganic precursor. HDA (Sigma Aldrich) is used as stabilizing agent. THF is collected from a solvent purification system (Braun MB-SPS-800). Distilled water has been degassed with argon during 30 min prior to use. In a typical experiment, to a THF (4 mL) solution of $[(Sn(NMe_2)_2]_2$ (0.5 mmol, 206.9 mg) mixed with HDA (0.05 mmol, 12 mg, 0.1 eq.), 2 mL of THF containing degassed distilled water (4 mmol, 72 µL, 8 eq.) is slowly added. After 16 h, the supernatant is removed by centrifugation (1000 rpm, 5 min, 20°C) and the precipitated powder is washed 3 times with 5 mL of acetone (Sigma Aldrich) in order to remove excess of organic ligands. The powder is then dried under low vacuum in a desiccator overnight. A white powder made of $Sn_3O_2(OH)_2$ is obtained as a final product.

Sensors preparation

$Sn_3O_2(OH)_2$ powder, at a concentration of 5 $mg.mL^{-1}$, has been dispersed in ethanol (Sigma Aldrich) using an ultrasonic bath (45 kHz, 10 min). The mixture has been drop-deposited on miniaturized gas sensors substrates by an ink-jet method (Autodrop AD system, Microdrop AG, Germany). The silicon platform of this study has been developed by the Laboratoire d'Analyse et d'Architecture des Systèmes, LAAS-CNRS, in the MICA group. The die size is 2×2 mm, and it integrates a 1.4 µm thick dielectric membrane (SiN_x/SiO_2) designed for an optimized thermal insulation of the heated area. A spiral shaped platinum heater is buried between the bottom dielectric membrane and the passivation top layer (silicon dioxide). This heater structure stands temperatures up to 700°C, and the power consumption is only as low as 55 mW at the operating temperature of 500°C. The interdigitated platinum electrodes for the measure of the sensitive layer are deposited as a final step on the top of the SiO_2 passivation layer and present a rounded shape. A distance of 10 µm between each electrode pole provides a reliable contact with the sensing layers.[17]

The sputtered SnO_2 thin film sensors are obtained from a commercial source. They are built on a micromachined silicon die (2.1x2.3 mm) with a thin dielectric membrane (2 µm thickness) which supports an integrated polysilicon heater (600 µm × 430µm). Two pairs of platinum electrodes are deposited to feed the heating resistance and to recover the signal of the sensitive layer (electrode poles distance *ca.* 300 µm).

Gas test set-up

Gas tests have been performed using a setup composed of different gas bottles connected to mass flow controllers (QualiFlow) commanded by an Agilent Data Acquisition/Switch Unit 34970A. Sensors are placed in a measurement cell equipped with humidity and temperature sensors. The integrated heaters are driven by a HP6642A tension controller. A National Instruments 6035E electronic card establishes the connection between a computing unit and the measurement cell. Freshly prepared sensitive layers are initially conditioned by a sequential *in situ* heating of the sensitive layer from ambient temperature to 500°C in air. Afterwards, the sensitive layer resistance is stabilized on the device by annealing at 500°C in synthetic air (relative humidity, RH 50%) at a total gas flow rate of 1 $L.min^{-1}$. Finally, the sensors are exposed to various controlled levels of CO, C_3H_8, NH_3, and NO_2. The tests reported here have been performed at operating temperatures of 500°C, 400°C, 340°C, and 300°C and at 50% RH. Resistance is measured before and after sensor exposure to reducing/oxidizing gas mixture, and the normalized responses to each gas is calculated as resistance variations, *i.e.* $Rn(\%) = (R_{air} - R_{gas})/R_{air}*100$, where R_{air} corresponds to the sensor resistance in synthetic air and R_{gas} corresponds to the sensor resistance in reducing/oxidizing gas mixture. Results reported here have been performed by using at least 3 sensors prepared as described above.

Characterization

The powder-diffraction patterns are obtained using SEIFERT XRD 3000 TT X Ray diffractometer with Cu-$K\alpha$ radiation, fitted with a diffracted-beam graphite monochromator. The data have been collected in the 2θ

configuration between 0 and 60°. Attenuated Total Reflection Infra-Red (ATR-IR) spectra are obtained by the direct deposition of a small amount of the $Sn_3O_2(OH)_2$ powder on a diamond crystal using Perkin-Elmer 100 spectrometer located in the glovebox under argon atmosphere. The spectra are registered between 4000 and 400 cm^{-1} wavenumber. Field Emission Scanning Electron Microscopy (FESEM) images are obtained using FEG FEI Quanta 250 microscope operating at 5 kV. Samples have been prepared by drop-deposition of the washed and dispersed in ethanol $Sn_3O_2(OH)_2$ powder, either on silica support or on miniaturized gas sensor substrates by an inkjet method as described above. Transmission Electron Microscopy (TEM) images are obtained using JEOL 1011 microscope operating at 100 kV. High-Resolution Transmission electron microscopy (HRTEM) are obtained using JEOL JSM 2100F microscope operating at 200 kV. TEM specimens have been prepared by drop deposition of bare $Sn_3O_2(OH)_2$ powder on a carbon-supported copper grids. The specific surface area has been determined by the Brunauer-Emmett-Teller (BET) method at 77 K using an ASAP2020 Physisorption Analyzer.

Acknowledgements

The work was financially supported by BPI France within the frame of Object's World ISI project. We thank our partners Sigfox SA. and Alpha-M.O.S. SA. We are grateful to Dr. Laure Vendier for X-rays diffraction analysis, and Vincent Collière for TEM and HRTEM microscopy. The authors thank CNRS and Université Fédérale de Toulouse, Université Paul Sabatier, for their support.

Keywords: • nanoparticles •hierarchical structures • metalorganic synthesis • SnO_2 • gas sensor

References

[1] C. Nayral, E. Viala, P. Fau, F. Senocq, J.-C. Jumas, A. Maisonnat, B. Chaudret, *Chem. Eur. J.* **2000**, 6, 4082-4090.
[2] M.-S. Park, G.-X. Wang, Y.-M. Kang, D. Wexler, S.-X. Dou, H.-K. Liu, *Angew. Chem. Int. Ed.* **2007**, 46, 750-753.
[3] E. R. Viana, J. C. Gonzalez, G. M. Ribeiro, A. G. de Oliveira, *J. Phys. Chem. C* **2013**, 117, 7844-7849.
[4] L. Shi, H. Lin, *Langmuir* **2011**, 27, 3977-3981.
[5] J. Ye, H. Zhang, R. Yang, X. Li, L. Qi, *Small* **2010**, 6, 296-306.
[6] H. Wang, A. L. Rogach, *Chem. Mater.* **2014**, 26, 123-133.
[7] P. Sun, X. Mei, Y. Cai, J. Ma, Y. Sun, X. Liang, F. Liu, G. Lu, *Sens. Actuators, B,* **2013**, 187, 301-307.
[8] H. Z. Wang, J. B. Liang, H. Fan, B. J. Xi, M. F. Zhang, S. L. Xiong, Y. C. Zhu, Y. T. Qian, *J. Solid State Chem.,* **2008**, 181, 122-129.
[9] Y. Li, L. Qiao, L. Wang, Y. Zeng, W. Fu, H. Yang, *Appl. Surf. Sci.* **2013**, 285, 130-135.
[10] N. G. Cho, D. J. Yang, M. J. Jin, H. G. Kim, H. L. Tuller, I. D. Kim, *Sens. Actuators B,* **2011**, 160, 1468-1472.
[11] N. Du, H. Zhang, J. Chen, J. Y. Sun, B. D. Chen, D. R. Yang, *J. Phys. Chem. B* **2008**, 112, 14836-14842.
[12] P. Wu, N. Du, H. Zhang, J. Yu, Y. Qi, D. Yang, *Nanoscale* **2011**, 3, 746-750.
[13] Q. Zhao, Y. Gao, X. Bai, C. Wu, Y. Xie, *Eur. J. Inorg. Chem.* **2006**, 8, 1643-1648.
[14] H. G. Yang, H. C., Zeng, *Angew. Chem. Int. Ed.* **2004**, 116, 6056-6059.
[15] J. Yin, X. Wang, R. Li, G. Wang, W. Zhang, *Mater. Lett.* **2013**, 113, 118-121.
[16] H. Wang, F. Fu. F. Zhang, H. E. Wang, S. V. Kershaw, J. Xu, S.-G. Sun, A. L. Roqach, *J. Mater. Chem.* **2012**, 22, 2140-2148.
[17] Ph. Menini, H. Chalabi, N. P. Yaboue, E. Scheid, V. Conedera, L. Salvagnac, K. Aguir, *Eurosensors XXII,* Dresde (Germany), September **2008**.
[18] M. L. Kahn, M. Monge, V. Collière, F. Senocq, A. Maisonnat, B. Chaudret, *Adv. Funct. Mater.* **2005**, 15, 458-468.
[19] A. Glaria, M. L. Kahn, P. Lecante, B. Barbara, B. Chaudret, *ChemPhysChem* **2008**, 9, 776-780.
[20] R. A. Ramik, R. M. Organ, J. A. Mandarino, *The Can. Mineral.* **2003**, 41, 649-657.
[21] H. B. Weiser, W. O. Milligan, *J. Phys. Chem.,* **1932**, 36, 3030-3038.
[22] J. Haines, J. M. Leger, *Phys. Rev. B,* **1997**, 55, 11144.
[23] J.-H. Lee, *Sens. Actuators B,* **2009**, 140, 319-336.
[24] Y. Coppel, G. Spataro, C. Pages, B. Chaudret, A. Maisonnat, M. L. Kahn, *Chem. Eur. J.* **2012**, 18, 5384-5393.
[25] R. L. Penn, J. F. Banfield, *Science* **2008**, 281, 969-971.
[26] C. Wang, G. Du, K. Stahl, H. Huang, Y. Zhong, J. Z. Jiang, *J. Phys. Chem. C,* **2012**, *116*, 4000-4011.
[27] H. Song, K.-H. Lee, H. Jeong, S. H. Um, G.-S. Han, H. S. Jung, G. Y. Jung, *Nanoscale* **2013**, *5*, 1188-1194.
[28] Z. Zhuang, X. Xue, Z. Lin, *Phys. Chem. Chem. Phys.* **2015**, *17*, 4845-4848.
[29] J. Khanderi, L. Shi, A. Rothenberger, *Inorg. Chim. Acta* **2015**, 427, 27-32.
[30] S. Zhang, H.-J. Sun, A. D. Hughes, R.-O. Moussodia, A. Bertin, Y. Chen, D. J. Pochan, P. A. Heiney, M. L. Klein, V. Percec, *PNAS* **2014**, 111, 9058-9063.
[31] X.G. Gong D. Y. Sun, X-Q. Wang, *Phys. Rev.B* **2000**, 62, 15420-15423.
[32] L. Y. Jiang, X. L. Wu, Y. G. Guo, L. J. Wan, *J. Phys. Chem. C* **2009**, 113, 14213-14219.
[33] A. Rothschild, Y. Komem, *J. Appl. Phys.* **2004**, 95, 6374-6380.
[34] C. Xu, J. Tamaki, N. Miura, N. Yamazoe, *J. Electrochem. Soc. Jpn.* **1990**, 58, 1143-1148; *Sens. and Actuators B* **1991**, 3, 147-155.
[35] J. Liu, X. Liu, Z. Zhai, G. Jin, Q. Jiang, Y. Zhao, C. Luo, L. Quan, *Sens. Actuators B*, **2015**, 220, 1354-1360.
[36] D. P. Volanti , A. A. Felix, M. O. Orlandi, G Whitfield , D.J. Yang , E. Longo , H. L. Tuller, J. A. Varela, *Adv. Funct. Mater.* **2013**, 23, 1759-1766.
[37] T. Kida, A. Nishiyama, Z. Hua, K. Suematsu, M. Yuasa, and K. Shimanoe, *Langmuir*, **2014**, 30, 2571-2579.
[38] P. Sun, W. Zhao, Y. Cao, Y. Guan, Y. Sun, G. Lu, *CrystEngComm* **2011**, 13, 3718-3724.
[39] J.-H. Lee, *Sens. Actuators B* **2012**, 140, 319-336.
[40] N. Barsan, C. Simion, T. Heine, S. Pokhrel, U. Weimar, *J. Electroceram.* **2010**, *25,* 11-19.